Published in final edited form as:
Microvasc Res. 2009 June ; 78(1): 132–139. doi:10.1016/j.mvr.2009.03.007.

Labeling of stem cells with monocrystalline iron oxide for tracking and localization by magnetic resonance imaging

Sergio Li Calzi[a], **David L. Kent**[b,c], **Kyung-Hee Chang**[a], **Kyle R. Padgett**[d], **Aqeela Afzal**[a], **Saurav B. Chandra**[d], **Sergio Caballero**[a], **Denis English**[e], **Wendy Garlington**[a], **Paul S. Hiscott**[b,c], **Carl M. Sheridan**[b,c], **Maria B. Grant**[a,*,1], and **John R. Forder**[d,f,g,1]

[a]Program in Stem Cell Biology, Department of Pharmacology and Therapeutics, University of Florida, Gainesville, FL, USA [b]Unit of Ophthalmology, Department of Medicine, University of Liverpool, UK [c]Eye Service, Aut Even Hospital, Kilkenny, Ireland [d]McKnight Brain Institute, University of Florida, Gainesville, FL, USA [e]Department of Neurosurgery, University of South Florida College of Medicine, USA [f]Department of Radiology, University of Florida, Gainesville, FL, USA [g]Department of Biomedical Engineering, University of Florida, Gainesville, FL, USA

Abstract

Precise localization of exogenously delivered stem cells is critical to our understanding of their reparative response. Our current inability to determine the exact location of small numbers of cells may hinder optimal development of these cells for clinical use. We describe a method using magnetic resonance imaging to track and localize small numbers of stem cells following transplantation. Endothelial progenitor cells (EPC) were labeled with monocrystalline iron oxide nanoparticles (MIONs) which neither adversely altered their viability nor their ability to migrate *in vitro* and allowed successful detection of limited numbers of these cells in muscle. MION-labeled stem cells were also injected into the vitreous cavity of mice undergoing the model of choroidal neovascularization, laser rupture of Bruch's membrane. Migration of the MION-labeled cells from the injection site towards the laser burns was visualized by MRI. In conclusion, MION labeling of EPC provides a non-invasive means to define the location of small numbers of these cells. Localization of these cells following injection is critical to their optimization for therapy.

Keywords

Stem cells; Cell localization; Cell therapy; In vivo tracking; Magnetic resonance imaging; Choroidal neovascularization; MION

Introduction

While stem cell therapy has succeeded in facilitating tissue regeneration and promoting healing, reproducible clinical benefits have remained elusive for reasons that have not yet been defined (Deans and Moseley, 2000; McKay, 2000; Pittenger et al., 1999). Studies by our group and others have demonstrated that very few stem cells localized within a precise target area are sufficient to accelerate tissue repair (Espinosa-Heidmann et al., 2003; Espinosa-Heidmann et al., 2005). On the other hand, other reports demonstrate that aberrant

*Corresponding author. Department of Pharmacology, University of Florida College of Medicine, 600 SWArcher Road, Box 100267, Gainesville, FL 32610, USA. Fax: +1 352 392 9696. grantma@ufl.edu (M.B. Grant).
[1]Contributed equally as senior authors of this manuscript.

localization of active stem cells can reduce therapeutic utility (Barbash et al., 2003). Given the additional, well established fact that hematopoietic stem cells (HSC) must migrate to areas of injury to initiate the repair process, the ability to track the migration of stem cells would greatly enhance their therapeutic utility. Moreover, because HSC and most other stem cell populations possess vast potential for self-replication, it is critical to be able to document the precise number of stem cell present, localize these cells and establish their viability after infusion. Therapeutic success will increase as methods are developed to optimize localization of infused cells and to direct infused stem cells to specific targets.

One stem cell population with marked clinical utility is bone marrow-derived stem cells (BMDC). These cells contribute to revascularization of wounds and damaged tissues. Numerous animal models have demonstrated the ability of transplanted marrow-derived progenitors to accelerate revascularization and promote healing after they home to sites of damage. Homing of these cells is influenced by numerous factors, including alterations in the extracellular environment and the presence of physical barriers such as disrupted tissues, neoplastic cells, scarring, and altered oxygen content. Moreover, loss of blood flow results in areas of ischemia which compromise the delivery of BMDC to sites of injury. As few as 5 stem cells within an area of 100 μm^2 readily accelerate tissue repair and provide as many as half of the cells that contribute to new vessel development (Chan-Ling et al., 2006; Harris et al., 2006).

To date, only a few methods (Shapiro et al., 2006; Heyn et al., 2006; Stroh et al., 2005) have been developed to localize very low numbers of engrafted stem cells. Thus novel strategies to detect small numbers of transplanted stem cell populations such as BMDC are greatly needed. Stem cells are often confined within a small but critical area before they avidly proliferate, differentiate, and finally assemble into functional tissues. The development of methods to localize these cells would help identify aberrant localization of transplanted stem cells. Here, we present a possible solution to this problem that employs high-field strength magnetic resonance imaging of stem cells pre-labeled with monocrystalline iron oxide.

Magnetic resonance imaging (MRI) is widely used in clinical settings due to its excellent soft-tissue contrast, high anatomical detail and minimal invasiveness. MRI sensitivity is improving by increasing signal-to-noise ratio (S/N) through use of higher magnetic field strengths, high performance gradients, and better radio frequency (RF) coils (Beck et al., 2002), all of which enable better resolution in a shorter time. High-field (≥3 T) MRI offers the advantage of noninvasive monitoring of transplanted cells with a resolution of 25 to 50 μm, approaching the size of single cells.

Transplanted cells must be labeled with a MR contrast agent in order to be visualized. Among the several MR contrast agents available, monocrystalline iron oxide nanoparticles (MION) have been successfully used for cell tracking *in vivo* (for review, see references Bjornerud and Johansson, 2004; Bulte and Kraitchman, 2004;Wu et al., 2004). MIONs are an attractive contrast agent because of their small size (5–30 nm) and because their cellular uptake occurs by adsorptive pinocytosis (Allen and Meade, 2003; Bulte et al., 2002; Dodd et al., 2001; Frank et al., 2003; Sundstrom et al., 2004; Weissleder, 1999; Weissleder and Mahmood, 2001), minimizing cell alterations.

In this report, we evaluated the utility of MION labeling for assessing the distribution of a well characterized human $CD133^+$, $CD14^-$, and $CD34^+$ stem cell population by MRI. We optimized the clinical applicability of our approach by not utilizing any agents to specifically enhance MION uptake by these cells. We assessed the effects of MION labeling on various aspects of cell function and used MRI to evaluate cell numbers and distribution.

Materials and methods

MION synthesis

MIONs were prepared as previously described (Kang et al., 1996) by mixing $FeCl_2$ and $FeCl_3$ solutions with NaOH solution yielding a precipitate of Fe_3O_4 (FeO/Fe_2O_3). The precipitate was collected via centrifugation and neutralized with HCl. Cationic colloidal nanoparticles were separated by centrifugation and stabilized with 1 M sodium citrate. Resultant MIONs were dialyzed against 0.1 M sodium citrate (pH 7.0) resulting in a brown transparent solution. The particle size of the MION preparation was determined by transmission electron microscopy (TEM), and was estimated to be approximately 4 nm. The iron concentration of MION solutionswas determined using a Cary 100 UV–Vis spectrophotometer. Solutions were acidified with HCl, buffered with sodium citrate (pH 4.0) and the iron was fully reduced to Fe^{2+} with 0.5 M hydroquinone. *o*-phenanthroline dye (20 mM) was used to form a colored complex with Fe^{2+} complex, and the iron concentration was calculated based on the absorbance measurement at 580 nm (Oca-Cossio et al., 2004).

Cell isolation and migration

The study protocol was approved by the institutional review board at the University of Florida, and written informed consent was obtained from each patient. Circulating stem cells were isolated from heparinized venous blood of healthy human donors as previously described (Segal et al., 2006). Briefly, for each patient 60 ml of blood were aseptically collected into heparinized glass vacuum tubes and then reacted with magnetic bead-conjugated anti-CD34 antibodies. For each assay a minimum of three patients' blood was pooled and separated according to manufacturer's directions (Stem Cell Technologies, Vancouver, BC, Canada). To test the influence of MION labeling on cell migration, 5000 stem cells were incubated in 2% fetal bovine serum-supplemented medium with 0, 5, 10, or 20 μM (0, 1:2000, 1:1000, or 1:500 dilution, respectively) of MIONs in 5% CO_2 at 37 °C overnight. After incubation, cells were stained with Calcein-AM (Molecular Probes, Carlsbad, CA), loaded onto the upper compartment of a Boyden migration chamber (Neuro Probe, Inc. Gaithersburg, MD) and induced to migrate through a 3 μm pore-size membrane towards either 10% FBS or 100 ng/ml stromal cell-derived factor-1 (SDF-1). PBS was used as negative control. After 4 h, the number of cells that migrated was determined by measuring fluorescence emitted at 550 nm when cells were exposed to light at an excitation frequency of 485±20 nm. Each sample was run in triplicate and results expressed as mean ±SD.

Cell viability and apoptosis

The effect of MION labeling on cell viability and apoptosis was tested using annexin V-FITC. Briefly, MION-labeled and unlabeled control cells were washed twice with cold PBS and resuspended in buffer at a concentration of 1×10^6 cells/ml. An aliquot (100 μl) of the solution was transferred to a new tube and incubated with 5 μl of Annexin V-FITC and 5 μl of propidium iodide (PI) to stain DNA. After gentle mixing, the cells were incubated for 15 min at room temperature (25 °C) after which the samples were analyzed by flow cytometry. Assays were performed in triplicate for each condition and results were calculated as the % of cells that took up annexin±SEM.

In vitro imaging

Nuclear magnetic resonance images were acquired using a wide bore (89 mm i.d.) 750 MHz magnet employing a Bruker Avance™ console. The RF power was adjusted to provide a 30° tip angle. The field of view was set at 19 mm×19 mm, and the matrix size was 512×400, to yield an in-plane resolution of 37 μm×48 μm. The slice thickness was set at 180 μm, the

repetition time was 1.7 s, the echo time was 15 ms, and the number of averages was 6. Total time for imaging was 1 h and 9 min, unless otherwise specified. To test the feasibility of imaging single MION-labeled cells, stem cells were labeled as described above and then dispersed at an extremely low density of approximately 200 cells/ml in 2% agarose gel in a 5 mm NMR glass tube (Wilmad Glass Co. Inc., Buena, NJ). The individual 5 mm vials were placed inside a 20 mm NMR tube along with two 5mmmarker vials. One marker vial contained a capillary tube and one was filled with Fluorinert™. These markers were used to ensure proper identification of the vials in post-processing. The agar samples were imaged using T2*-weighted gradient echo imaging techniques.

In order to provide direct evidence that the areas of decreased image intensity corresponded to MION located within labeled stem cells, cells were plated on fibronectin-coated coverslips and examined using MRI and light microscopy. Peripheral blood mononuclear cells (PBMCs) were isolated from fresh blood by light density separation using Ficoll-Paque™ PLUS (StemCell Technologies, Inc.) and cultured on fibronectin-coated plates for 2 days (negative selection) at 37 °C in 5% CO_2 in EndoCult medium (StemCell Technologies, Inc.). The stem cell-containing supernatants were then transferred to culture dishes in which fibronectin-coated coverslips were placed. When the cells reached 60% confluence, they were incubated with various concentrations of MION (final concentrations 5, 10, and 20 μM) overnight at 37 °C. The following day coverslips were washed three times in PBS to remove unincorporated MION then fixed in 4% paraformaldehyde pH 7.4 for 10 min at room temperature and washed three additional times in PBS. Parameters used for the imaging were as follows: 25×25 mm field of view; matrix size 256×256; 100 μm slice thickness; repetition time 5 s; echo time 15 ms; number of averages was 4, and the total time for imagingwas 1 h and 25 min. Our in-plane resolution was 98 μm×98 μm, resulting in virtually isotropic voxel dimensions. We used a gradient echo pulse sequence to enhance our ability to detect alterations in T2*. Unlabeled cells were used as a negative control. Following MR imaging, coverslips were stained with Prussian Blue, as described below, for iron detection.

To test the long-term effect of intracellular MION on cell growth in culture, stem cells were observed for up to 16 days after labeling and photographed at day 3 and 16 on a Zeiss Axiovert 200 optical microscope and compared with unlabeled cells at the same times.

Detection of MION-labeled stem cells in mouse hind limb

C57BL/6J mice were obtained from The Jackson Laboratory (Bar Harbor, ME). Hind limbs were injected intramuscularly at three sites with specific numbers of MION-labeled circulating $CD34^+$ cells from pooled healthy human donors (Lonza, Rockland, ME), 5, 50, and 500, as indicated, suspended in 50 μl of saline. Sham injection (50 μl saline only) was added as control. Imaging was performed on three mice, approximately 1 h post-injection. Datasets were collected on a 11.1 T magnet employing a Bruker Avance console using a gradient echo sequence to enhance detection perturbations in T2. The field of view was 2 cm×1.2 cm, and a 256×128 matrix was employed, yielding an in-plane resolution of 78 μm×94 μm. The tissue slice thickness was 700 μm and the repetition time was 300 ms. Echo time ranged from 5 ms to 15 ms in 1 ms increments. Flip angle was 30°. Two days post-imaging, mice were sacrificed and hind limbs fixed in 4% paraformaldehyde for histological analysis as described below.

Immunofluorescence staining of MION-labeled stem cells

Mouse hind limb or mouse eye paraffin sections (5 μm) were deparaffinized in xylene, rehydrated in a graded ethanol series and then incubated with Mouse on Mouse (M.O.M™) immunodetection kit (Vector Laboratories Inc., Burlingame, CA), following the

manufacturer's directions, and either a mouse anti-human CD34 antibody (Abcam Inc., Cambridge, MA) in a 1:500 dilution or a mouse anti-human nuclear antigen antibody (Millipore, Billerica, MA) in a 1:20 dilution. Sections were then mounted with Vectashield® 4′, 6-diamino-2-phenylindole (DAPI) (Vector) for DNA labeling and examined using a fluorescence microscope (ZEISS Axiovert 200) using a W-PI 10×/23 ocular and a LD Plan Neofluar 40×/0.6 Ph2 objective. Pictures were captured using a ZEISS Axiocam MRm digital camera and processed using Axiovision Rel. 4.4 for Windows.

Prussian blue staining of MION-labeled stem cells

MION-labeled stem cells were detected in fibronectin-coated coverslips and in paraffin sections using ACCUSTAIN® Iron Stain (Sigma-Aldrich® HT20-1KT) following the manufacturer's protocol.

Choroidal neovascularization (CNV) mouse model

C57BL/6J mice (n=3/condition) (wild type, WT) (Jackson Laboratory) 6–8 weeks of age, were treated with laser photocoagulation in a manner similar to that used by Ryan (1979) and previously described (Sengupta et al., 2003). Briefly, each eye received three laser burns to rupture Bruch's membrane, resulting in a bubble over the ruptured area. The right eye of either laser injured or non-injured animals were intravitreally injected with 50,000 human $CD133^+$, $CD14^-$, and $CD34^+$ MION-labeled stem cells resuspended in 2 μl saline while corresponding left eyes were injected with unlabeled stem cells or saline. All animalswere imaged at 24 and 48 h after laser injury and stem cell injection. At the time of euthanasia, the eyes were enucleated and incubated in 4% paraformaldehyde for 1 h and rinsed in PBS for 30 min before paraffin embedding.

Monitoring of stem cell in ocular tissue

All datasets were collected on a 17.6 T magnet employing a Bruker Avance console.

For *ex vivo* studies, mouse eyes were placed in 4% paraformaldehyde for 30 min and then in phosphate buffered saline (PBS) overnight at 4 °C. The eye was then immersed in Fluorinert™ (3 M, St. Paul, MN), a susceptibility matched fluorine solution, and then placed in a 5 mm diameter custom built coil. High resolution 3D gradient echo (GE) imaging was employed to enhance anatomical detail. The MR parameters used were a matrix of 200×180×80 μm, a bandwidth of 19 kHz, a TR of 500 ms, a TE of 7.5 ms, and a field of view of 0.38×0.38×0.38. Results from 6 separate experiments were assessed. For *in vivo* studies, mouse eyes were intravitreally injected with 50,000 circulating $CD34^+$ cells from pooled healthy human donors (Lonza) resuspended in 2 μl saline solution. Mice were imaged at 24 and 48 h post-injection. We used a linear square surface coil with dimensions 1 cm×1 cm. It has individual capacitive adjustments for tune and match. The overall *in vivo* setup included respiration monitoring, anesthesia and heating pads for the mice. The parameters used were TR=5000 ms, TE=10 ms, matrix size=512×256, FOV=1.2×0.9 and slice thickness=0.25 mm. The following day, mice were sacrificed and eyes enucleated and fixed in 4% paraformaldehyde for histological examination.

Statistical analyses

Results are expressed as mean±SEM and are derived from at least three independent experiments. Data were analyzed by analysis of variance (ANOVA). Each concentration was compared with control levels; differences were considered significant when $p<0.05$.

Results

Effect of MION on viability, morphology and migration of stem cells

The effect of MION labeling on cell viability and apoptosis was tested by assessing the uptake of FITC-labeled annexin V. MION labeling did not adversely impact stem cells viability or death although an increase in early apoptosis was observed at higher concentrations (Fig. 1). The high cell death rate observed in all the samples is a common phenomenon and is due to cell manipulation. To asses the effect of MION labeling on cell morphology, stem cells cultured for 5 days were incubated with 20 μM MION (1:500 dil.) and maintained in culture for another 16 days. During this time cells were examined microscopically. After 3 days, control cells and MION-labeled cells appeared indistinguishable. However, 16 days after labeling, both groups started to manifest some morphologic differences (data not shown).

Stem cells were incubated with 5 μM, 10 μM, or 20 μMof MION and their migration was compared to that of unlabeled cells. MION labeling did not alter migratory responses of the cells to either fetal bovine serum (Fig. 2) or to stromal derived factor-1 (SDF-1, not shown). In addition, MION labeling did not alter responses of cells not exposed to chemoattractants.

In vitro imaging

MION-labeled stem cells were dispersed at a concentration of approximately 200 cells/ml in 2% agar gel and poured into 5mmNMR glass tubes for imaging (Figs. 3A and B). Small areas within the gel were characterized by a decrease in image intensity, consistent with the presence of MION. Since the dispersion of the cells in agar was 200 cells/ml and the volume of a given voxel is 0.32 nL, it is unlikely that more than 1–2 cells will contribute to image intensity decrease.

To confirm that MION was indeed intracellular, and that intracellular MION could be detected by MRI, stem cells were cultured on fibronectin-coated coverslips and allowed to differentiate, and therefore adhere, before being labeled overnight with MION. Cell differentiation and attachment served two valuable purposes: 1) they allowed extensive washes without cell loss for non-internalized MION particle removal, confirmed by microscopic examination of Prussian Blue-stained cells (see below), and 2) provided evidence for maintenance of MION labeling capability after cell differentiation. When these cells were examined by MRI as described above, all MION-labeled samples showed areas of decreased image intensity (Figs. 3C, D). Prussian blue staining confirmed the exclusive presence of intracellular iron in MION-labeled stem cells (Figs. 3E, F).

In vivo imaging of stem cells injected into murine hind limb

The hind limb of a mouse was injected with varying numbers of MION-labeled stem cells and multi-slice gradient echo images were obtained at echo times ranging from 5 to 15 ms using a 11.1 T Bruker NMR spectrometer. Areas of decreased signal intensity in the images were attributed to MION accumulation if the decrease in signal intensity was more evident with increased echo time due to increased T2* effects. As shown in Fig. 4A, three areas of decreased image intensity were observed in the hind limb. These areas were representative of either approximately 5, 50, or 500 cells, respectively. A mock injection control was also included and showed no signal void (data not shown). Histological analyses confirmed the presence of iron (Fig. 4E) in human stem cells (Fig. 4F). Since the lowest concentration injected was approximately 5 cells, this suggested that at a field strength of 11.1 T, sufficient signal exists to detect small quantities of MION-labeled cells using MR imaging.

Imaging of stem cells in murine eyes

Ex vivo imaging of an enucleated mouse eye at 17.6 T clearly demonstrated all the layers of the retina and posterior pole (Fig. 5). While it is widely accepted that endothelial precursors participate in the formation of choroidal neovascularization (CNV), it is not known if their contribution is beneficial or deleterious. To take a first step towards answering this question using MR imaging, mouse eyes were injured with 3 laser burns to the Bruch's membrane and MION-labeled cells were injected within the vitreous. Imaging these mice *in vivo* 24 and 48 h post-injection demonstrated the movement of cells from the edge of the lens to the posterior region of the eye and their movement through the retina toward the area of injury (Fig. 6). Histological examination of mouse retina sections detected MION-labeled cells (Figs. 7 and 8) and confirmed their human origin (Fig. 8). These cells are viable and labeling appears to be maintained after cell division (Fig. 8C). Thus MR imaging of stem cells was effective in tracking the cells *in vivo* and should provide a means to optimize localization of infused stem cells.

Discussion

Stem and progenitor cell therapies have shown success in regeneration and repair of damaged tissue, but one difficulty encountered in optimizing these techniques is the inability to follow the fate of the transplanted stem cells in the recipients (Daldrup-Link et al., 2005). To date, a wide spectrum of *in vivo* cell-tracking techniques are available. However, all have limitations usually associated with inadequate contrast and potential radiation damage. While the use of scintigraphic techniques to track labeled cells provides increased sensitivity in isolated tissue (Kiessling, 2008; Thompson et al., 2005), these techniques do not provide the spatial resolution that is possible with high-field MR, (Badea et al., 2008; Herschman, 2003). Reporter genes, while providing much greater sensitivity for identifying labeled cells, generally lack spatial specificity for *in vivo* detection. MR imaging is well-suited for this task, because it can enable both whole-body examinations and subsequent detailed depictions of host organs with near-microscopic anatomic resolution and excellent soft-tissue contrast. In addition, MR imaging allows repetitive investigations without known side effects and without risking radiotoxic damage to the transplanted cells. However, to visualize and track stem and progenitor cells, they must be labeled with MR imaging contrast agents. The development of dedicated labeling techniques has been investigated (Bulte and Kraitchman, 2004; Crich et al., 2004; Winnard and Raman, 2003). Cell-labeling techniques are restricted by the concentration of internalized contrast agent which limits sensitivity for detection by MRI. This constraint can be overcome by using very high magnetic field strengths (Lewin et al., 2000).

In both experimental and clinical settings, cellular MRI offers the advantage of non-invasive monitoring of the distribution of transplanted cells in real time at a resolution of less than 25 to 50 μm, a size that approaches the goal of identification of a single cell. Among the several MRI contrast agents available, MIONs have been successfully used to magnetically label cells (Bjornerud and Johansson, 2004; Bulte and Kraitchman, 2004;Wu et al., 2004). They are our contrast agent of choice because of their small size (5 to 30 nm) and because, in stem cells, MION are internalized without use of transfection agents or other agents that disrupt cell membranes.

Both particle size and coating (citrate, carboxydextran, or others) impact the route (pinocytotic, phagocytotic, etc.) and efficacy of uptake in different cell lines (for a review, see Rogers et al., 2006). The optimal choice for labeling of a particular type of cell will be dependent upon these factors and the requisite sensitivity that is needed. The particles we used were comprised of a 4 nm iron oxide core with an anionic citrate coating, resulting in a hydrodynamic diameter of approximately 8 nm. Paramagnetic iron oxide particles in use for

magnetic resonance contrast range from ultrasmall superparamagnetic iron oxide (USPIO; <40 nm) to superparamagnetic iron oxide (SPIO; usually characterized as 100–300 nm) to micrometer-sized particles (MPIO; ≥1 μm). The purpose of the present study was to evaluate the effects on cell viability and sensitivity for detection of one species of iron oxide contrast agent — one which has been identified in previous studies to permit detection of small numbers of cells (Heyn et al., 2006; Stroh et al., 2005).

Susceptibility-based detection methods, especially with paramagnetic agents, result in local field perturbations that are reflected by regions of decreased image density that may extend far beyond the image location of the agent itself. In the case of the *in vitro* experiments reported here, we sought to minimize this problem by serial dilution of the cell suspensions to yield very low density in both the agar and coverslip preparations. Moreover, the choice of echo time (15 ms) at this field (17.6 T) was chosen to maintain spatial information (i.e., longer echo times resulted in much larger areas of decreased image intensity). Combined with validation by light microscopy on the same coverslip preparations, we are confident that we have detected single cells labeled with MION at this field.

Here, we show for the first time that MION labeling, using this preparation, did not reduce viability of human stem cells; however, at higher MION concentrations, we observed an increase in early apoptosis. *In vitro* cell migration and behavior in short term culture was indistinguishable from that of unlabelled cells. Furthermore, we demonstrate *in vitro* the detection of MION within single stem cells while, *in vivo*, we found that very small numbers of stem cells could easily be localized by this method. Successful stem cell therapy is likely to depend on the localization of small numbers of cells, therefore the results we present are of particular importance. These results support that MRI represents a technique that offers the advantage of non-invasively monitoring a small number of stem cells which is essential for precise definition of the distribution of injected cells, an endeavor which will allow optimization of stem cell therapy and answer key questions that may explain the failure and inconsistent results reported in many studies undertaken to date. Moreover, since stem cells possess a tremendous ability to self replicate, it is important that they are transplanted in the correct location. Thus, strategies to localize stem cells have great therapeutic significance. The method we report will allow realization of that goal. In our study, we employed a stem cell population that is known to differentiate into endothelial cells and directly revascularize areas of injury as well as provide a source of paracrine factors that promote vessel repair as well as maintain vascular health. EPC display a potential for repair of damaged vasculature, a major cause of morbidity and devastating pathology in eyes and other organs. The ability of these cells to migrate to the area where they are needed for repair is often altered in disease states that led to the initial damage, such as diabetic retinopathy, wounding or infection.

Using a well-defined model of vascular eye injury previously developed in our labs, we successfully employed MRI to assess the migration of stem cells within the eye as they homed to foci of injury where they can facilitate vascular repair (Grant et al., 2002). These results confirm our conclusion that MR imaging of stem cells is extremely effective in tracking the distribution and subsequent migration of stem cells in a delicate therapeutic setting, and will provide a means to allow further optimization of the localization of infused stem cells. Furthermore, data in the hind limb model reported herein support our contention that a very small number of human stem cells, perhaps as fewas 5 cells, can be detected *in vivo* by this approach. Future applications of this technology may include *in vivo* monitoring of newcell-based therapies, such as homing ofmesenchymal stem cells in injured myocardium, homing of neurologic stem cells in impaired brain tissue, and evaluation of revascularized ischemic limbs. Specifically, MION-labeled stem cellsmay be used in the future tomonitor the therapeutic success of revascularization in the myocardium and

extremities. Furthermore, due to its high level of safety for human subjects, high-field MRI is becoming optimum clinical standard in both the US and Europe. The recent decision by the United States Food and Drug Administration (FDA) to remove the investigational approval requirement for fields ≤8 T reflects this trend.

In conclusion, iron oxide-labeled human stem cells show excellent viability and function and can be detected non-invasively *in vivo* with submillimeter anatomic resolution by using 11 T MR imaging equipment demonstrating that this cell-tracking technique has clinical applicability. MION may provide biological insights relevant for the development of newcell-based therapies and may be generally suited to monitor stem cell homing and engraftment in patients.

Acknowledgments

The authors express their sincere gratitude to the late Dr. Ioannis Constantinidis who provided essential materials used to complete this study. The authors wish to express their gratitude to Dr. Lynn C. Shaw for his outstanding graphic contribution. This research was supported by a program project grant from the Juvenile Diabetes Research Foundation awarded to Drs. Grant and Forder, by National Institutes of Health grants EY012601, EY007739 R21 and EY14818 awarded to Dr. Grant, and by the American Heart Association grants 0625533B and 0865213E awarded to Dr. Li Calzi.

References

Allen MJ, Meade TJ. Synthesis and visualization of a membrane-permeable MRI contrast agent. J Biol Inorg Chem. 2003; 8:746–750. [PubMed: 14505078]

Badea CT, Drangova M, Holdsworth DW, Johnson GA. In vivo small-animal imaging using micro-CT and digital subtraction angiography. Phys Med Biol. 2008; 53:R319–350. [PubMed: 18758005]

Barbash IM, Chouraqui P, Baron J, Feinberg MS, Etzion S, Tessone A, Miller L, Guetta E, Zipori D, Kedes LH, Kloner RA, Leor J. Systemic delivery of bone marrow-derived mesenchymal stem cells to the infarcted myocardium: feasibility, cell migration, and body distribution. Circulation. 2003; 108:863–868. [PubMed: 12900340]

Beck B, Plant DH, Grant SC, Thelwall PE, Silver X, Mareci TH, Benveniste H, Smith M, Collins C, Crozier S, Blackband SJ. Progress in high field MRI at the University of Florida. Magma. 2002; 13:152–157. [PubMed: 11755090]

Bjornerud A, Johansson L. The utility of superparamagnetic contrast agents in MRI: theoretical consideration and applications in the cardiovascular system. NMR Biomed. 2004; 17:465–477. [PubMed: 15526351]

Bulte JW, Kraitchman DL. Iron oxide MR contrast agents for molecular and cellular imaging. NMR Biomed. 2004; 17:484–499. [PubMed: 15526347]

Bulte JW, Duncan ID, Frank JA. In vivo magnetic resonance tracking of magnetically labeled cells after transplantation. J Cereb Blood Flow Metab. 2002; 22:899–907. [PubMed: 12172375]

Chan-Ling T, Baxter L, Afzal A, Sengupta N, Caballero S, Rosinova E, Grant MB. Hematopoietic stem cells provide repair functions after laser-induced Bruch's membrane rupture model of choroidal neovascularization. Am J Pathol. 2006; 168:1031–1044. [PubMed: 16507916]

Crich SG, Biancone L, Cantaluppi V, Duo D, Esposito G, Russo S, Camussi G, Aime S. Improved route for the visualization of stem cells labeled with a Gd-/Eu-chelate asdual (MRI and fluorescence) agent. Magn Reson Med. 2004; 51:938–944. [PubMed: 15122675]

Daldrup-Link HE, Rudelius M, Piontek G, Metz S, Brauer R, Debus G, Corot C, Schlegel J, Link TM, Peschel C, Rummeny EJ, Oostendorp RA. Migration of iron oxide-labeled human hematopoietic progenitor cells in a mouse model: in vivo monitoring with 1.5-T MR imaging equipment. Radiology. 2005; 234:197–205. [PubMed: 15618382]

Deans RJ, Moseley AB. Mesenchymal stem cells: biology and potential clinical uses. Exp Hematol. 2000; 28:875–884. [PubMed: 10989188]

Dodd CH, Hsu HC, Chu WJ, Yang P, Zhang HG, Mountz JD Jr, Zinn K, Forder J, Josephson L, Weissleder R, Mountz JM, Mountz JD. Normal T-cell response and in vivo magnetic resonance

imaging of T cells loaded with HIV transactivator-peptide-derived superparamagnetic nanoparticles. J Immunol Methods. 2001; 256:89–105. [PubMed: 11516758]

Espinosa-Heidmann DG, Caicedo A, Hernandez EP, Csaky KG, Cousins SW. Bone marrow-derived progenitor cells contribute to experimental choroidal neovascularization. Invest Ophthalmol Vis Sci. 2003; 44:4914–4919. [PubMed: 14578417]

Espinosa-Heidmann DG, Reinoso MA, Pina Y, Csaky KG, Caicedo A, Cousins SW. Quantitative enumeration of vascular smooth muscle cells and endothelial cells derived from bone marrow precursors in experimental choroidal neovascularization. Exp Eye Res. 2005; 80:369–378. [PubMed: 15721619]

Frank JA, Miller BR, Arbab AS, Zywicke HA, Jordan EK, Lewis BK, Bryant LH Jr, Bulte JW. Clinically applicable labeling of mammalian and stem cells by combining superparamagnetic iron oxides and transfection agents. Radiology. 2003; 228:480–487. [PubMed: 12819345]

Grant MB, May WS, Caballero S, Brown GA, Guthrie SM, Mames RN, Byrne BJ, Vaught T, Spoerri PE, Peck AB, Scott EW. Adult hematopoietic stem cells provide functional hemangioblast activity during retinal neovascularization. Nat Med. 2002; 8:607–612. [PubMed: 12042812]

Harris JR, Brown GA, Jorgensen M, Kaushal S, Ellis EA, Grant MB, Scott EW. Bone marrow-derived cells home to and regenerate retinal pigment epithelium after injury. Invest Ophthalmol Vis Sci. 2006; 47:2108–2113. [PubMed: 16639022]

Herschman HR. Micro-PET imaging and small animal models of disease. Curr Opin Immunol. 2003; 15:378–384. [PubMed: 12900267]

Heyn C, Ronald JA, Mackenzie LT, MacDonald IC, Chambers AF, Rutt BK, Foster PJ. In vivo magnetic resonance imaging of single cells in mouse brain with optical validation. Magn Reson Med. 2006; 55:23–29. [PubMed: 16342157]

Kang YS, Risbud S, Rabolt JF, Stroeve P. Synthesis and characterization of nanometer-size Fe3O4 and γ-Fe2O3 particles. Chem Mater. 1996; 8:2209–2211.

Kiessling F. Noninvasive cell tracking. Handb Exp Pharmacol. 2008:305–321. [PubMed: 18626608]

Lewin M, Carlesso N, Tung CH, Tang XW, Cory D, Scadden DT, Weissleder R. Tat peptide-derivatized magnetic nanoparticles allow in vivo tracking and recovery of progenitor cells. Nat Biotechnol. 2000; 18:410–414. [PubMed: 10748521]

McKay R. Stem cells—hype and hope. Nature. 2000; 406:361–364. [PubMed: 10935622]

Oca-Cossio J, Mao H, Khokhlova N, Kennedy CM, Kennedy JW, Stabler CL, Hao E, Sambanis A, Simpson NE, Constantinidis I. Magnetically labeled insulin-secreting cells. Biochem Biophys Res Commun. 2004; 319:569–575. [PubMed: 15178444]

Pittenger MF, Mackay AM, Beck SC, Jaiswal RK, Douglas R, Mosca JD, Moorman MA, Simonetti DW, Craig S, Marshak DR. Multilineage potential of adult human mesenchymal stem cells. Science. 1999; 284:143–147. [PubMed: 10102814]

Rogers WJ, Meyer CH, Kramer CM. Technology insight: in vivo cell tracking by use of MRI. Nat Clin Pract Cardiovasc Med. 2006; 3:554–562. [PubMed: 16990841]

Ryan SJ. The development of an experimental model of subretinal neovascularization in disciform macular degeneration. Trans Am Ophthalmol Soc. 1979; 77:707–745. [PubMed: 94717]

Segal MS, Shah R, Afzal A, Perrault CM, Chang K, Schuler A, Beem E, Shaw LC, Li Calzi S, Harrison JK, Tran-Son-Tay R, Grant MB. Nitric oxide cytoskeletal-induced alterations reverse the endothelial progenitor cell migratory defect associated with diabetes. Diabetes. 2006; 55:102–109. [PubMed: 16380482]

Sengupta N, Caballero S, Mames RN, Butler JM, Scott EW, Grant MB. The role of adult bone marrow-derived stem cells in choroidal neovascularization. Invest Ophthalmol Vis Sci. 2003; 44:4908–4913. [PubMed: 14578416]

Shapiro EM, Sharer K, Skrtic S, Koretsky AP. In vivo detection of single cells by MRI. Magn Reson Med. 2006; 55:242–249. [PubMed: 16416426]

Stroh A, Faber C, Neuberger T, Lorenz P, Sieland K, Jakob PM, Webb A, Pilgrimm H, Schober R, Pohl EE, Zimmer C. In vivo detection limits of magnetically labeled embryonic stem cells in the rat brain using high-field (17.6 T) magnetic resonance imaging. Neuroimage. 2005; 24:635–645. [PubMed: 15652299]

Sundstrom JB, Mao H, Santoianni R, Villinger F, Little DM, Huynh TT, Mayne AE, Hao E, Ansari AA. Magnetic resonance imaging of activated proliferating rhesus macaque T cells labeled with superparamagnetic monocrystalline iron oxide nanoparticles. J Acquir Immune Defic Syndr. 2004; 35:9–21. [PubMed: 14707787]

Thompson M, Wall DM, Hicks RJ, Prince HM. In vivo tracking for cell therapies. Q J Nucl Med Mol Imaging. 2005; 49:339–348. [PubMed: 16407817]

Weissleder R. Molecular imaging: exploring the next frontier. Radiology. 1999; 212:609–614. [PubMed: 10478223]

Weissleder R, Mahmood U. Molecular imaging. Radiology. 2001; 219:316–333. [PubMed: 11323453]

Winnard P Jr, Raman V. Real time non-invasive imaging of receptor–ligand interactions in vivo. J Cell Biochem. 2003; 90:454–463. [PubMed: 14523979]

Wu EX, Tang H, Jensen JH. Applications of ultrasmall superparamagnetic iron oxide contrast agents in the MR study of animal models. NMR Biomed. 2004; 17:478–483. [PubMed: 15526349]

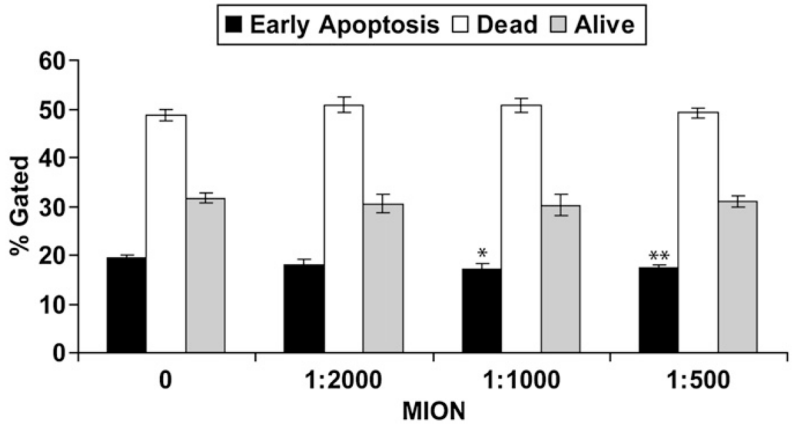

Fig. 1.

MION labeling does not affect stem cell viability and apoptosis: stem cells were incubated overnight with increasing concentrations of MION and apoptosis was measured the following day by FACS as described. Shown are representative results of 3 different experiments performed in triplicate as % gated±SEM. **P*=0.03; ***P*=0.007.

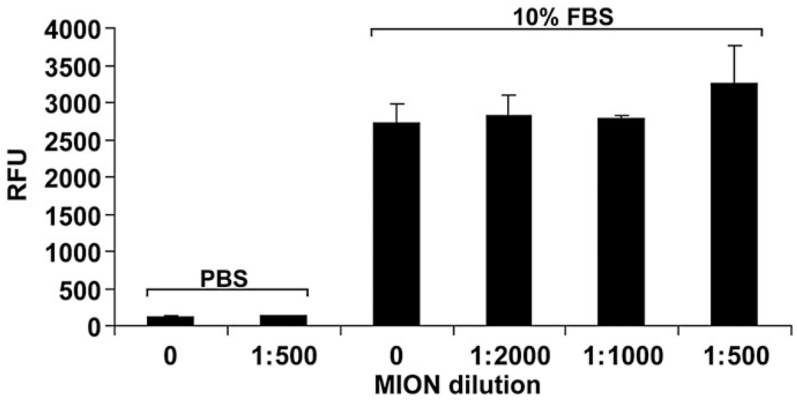

Fig. 2.

MION labeling does not affect cell migration. Increasing concentrations (expressed as dilutions) of MION were used to label stem cells. Cells were then challenged to migrate towards either 10% FBS or PBS (negative control). Shown are representative results of 3 different experiments performed in triplicate as relative fluorescence units (RFU)±SEM. No intra-group significance was observed. Inter-group $P<0.05$.

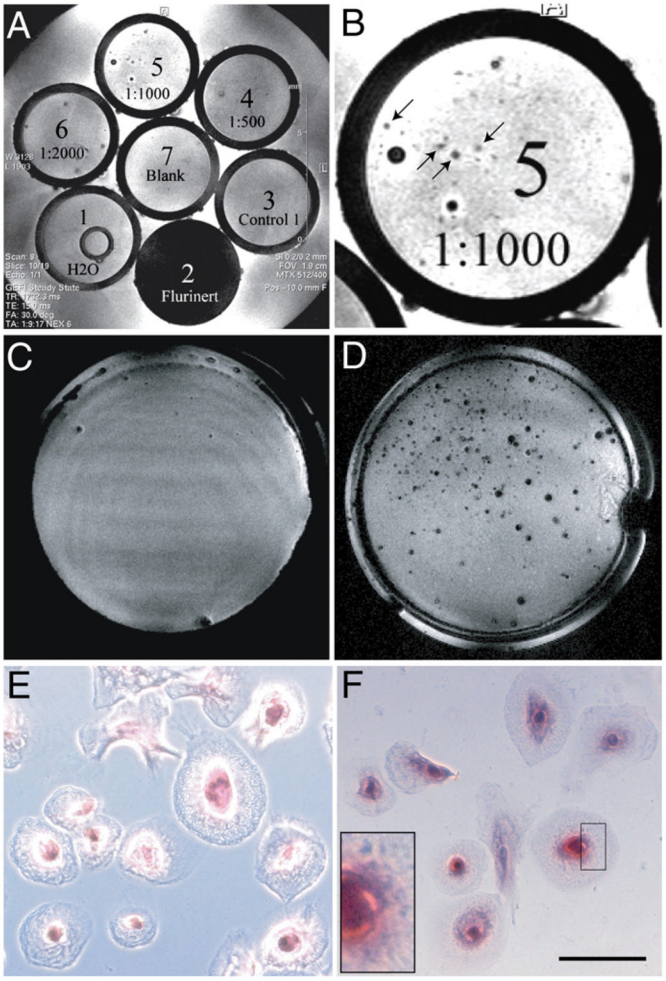

Fig. 3.

MION labeling allows imaging of a single stem cell *in vitro*. A: Stem cells were labeled with increasing concentrations of MION (as indicated), dispersed in 2% agar, and placed in NMR tubes for imaging. Blank: agar alone. Control 1: unlabeled cells. Fluorinert and H_2O were used as controls for MRI. Shown is a representative slice through the tubes. B: Close-up of tube # 5 in panel A. MION-labeled cells are indicated (arrows). The larger dark spots represent air bubbles that formed during agar solidification. C and D: Stem cells cultured on fibronectin-coated coverslips were incubated in medium without (C) or in the presence of (D) MION overnight. After extensive washes to remove non-internalized MION, samples were fixed in 4% paraformaldehyde and then imaged as described. Small areas within the coverslip were characterized by a decrease in image intensity, consistent with the presence of MION (D). E and F: The same samples shown in panels C and D, where stained for iron (Prussian Blue). E: Control, F: MION-labeled cells. Inset shows intracellular iron particles (blue). Scale bar is 10 μm.

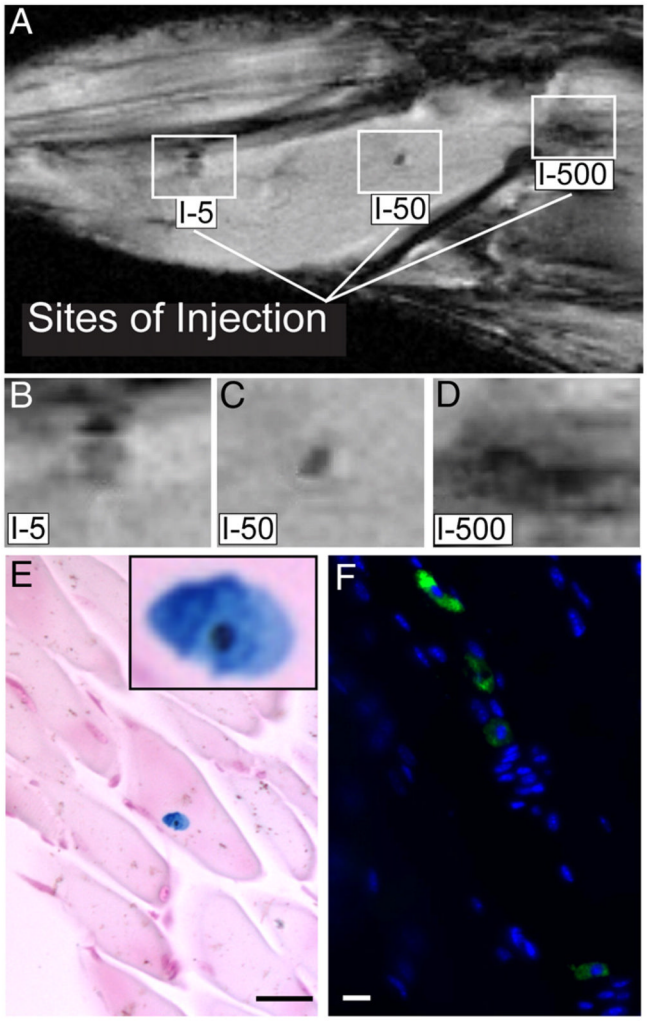

Fig. 4.

In vivo MRI of hind limb of mouse injected with MION-labeled human stem cells. Varying numbers of MION-labeled human stem cells (5, 50 or 500 cells) were injected intramuscularly in the hind limb of a mouse. In the top panel (A), limbs were imaged using a Bruker 11.1 T/40 cm wide bore NMR spectrometer. The lines point to dark areas where the indicated numbers of MION-labeled stem cells were injected. High magnification of the injection sites are shown in panel (B, C, and D). In panel (E) is a representative image of a single MION-labeled cell detected in a paraffin-embedded muscle section using Prussian Blue staining. Inset shows the MION-labeled cell at higher magnification. In panel (F), injected cells were identified in a paraffin-embedded section using anti-human CD34 antibody (green) and DAPI (blue). A representative fluorescence image is shown. I-5=Injected 5 cells. Scale bars are 3 μm.

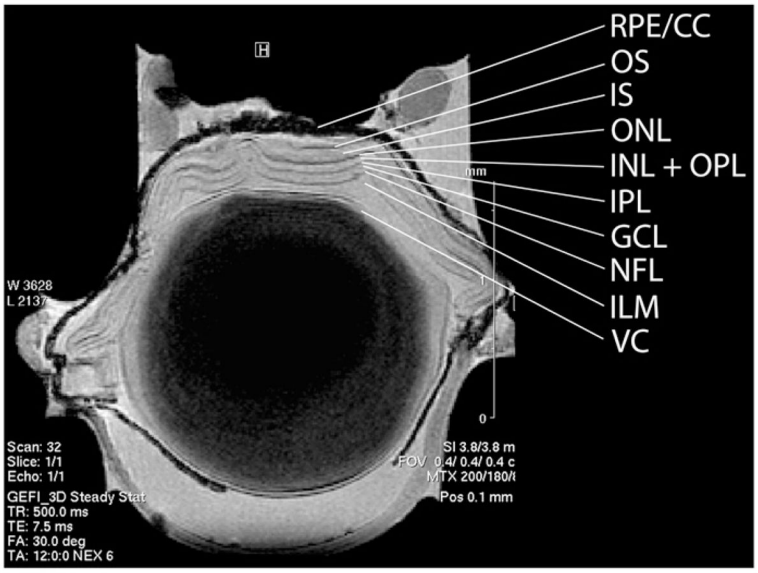

Fig. 5.

Ex vivo imaging of a mouse eye. Mouse eyes were enucleated, fixed and imaged at high resolution on a 17.6 T magnet. Layers of the retina were identified. VC=vitreal chamber, ILM=inner limiting membrane, NFL=nerve fiber layer, GCL=ganglion cell layer, IPL=inner plexiform layer, OPL=outer plexiform layer, INL=inner nuclear layer, ONL=outer nuclear layer, IS=inner segments, OS=outer segments, RPE=retinal pigment epithelium, CC=choroid capillaries.

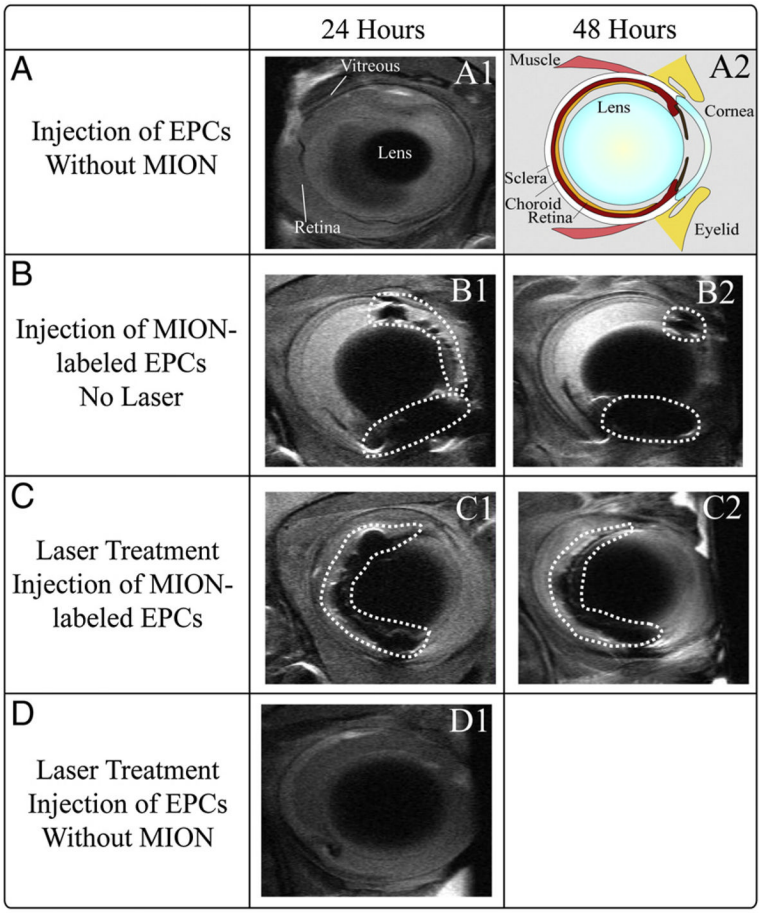

Fig. 6.

In vivo tracking of stem cells injected in a mouse eye. A1: Mouse eye intravitreally injected with unlabeled stem cells and imaged by MRI at 24 h following injection. A2: Schematic of a mouse eye. B1 and B2: The MION-labeled cells are localized to the edge of the lens more anterior in the uninjured eye, 24 h (B1) and 48 h (B2) following injection. C1 and C2: Intravitreal injection of MION-labeled stem cells into mouse eyes that underwent rupture of Bruch's Membrane (3 burns) and imaged by MRI 24 h (C1) and 48 h (C2) following lasering. The MION-labeled cells are localized to the edge of the lens in the posterior region of the eye beginning to incorporate into the retina and traversing the retina toward the area of injury. B1 and B2, as well as C1 and C2, represent images of the same mouse at the indicated time points. D1: Intravitreal injection of unlabeled $CD34^{+}$ cells into a mouse eye 24 h following injection. Dotted circles enclose MION-labeled cells.

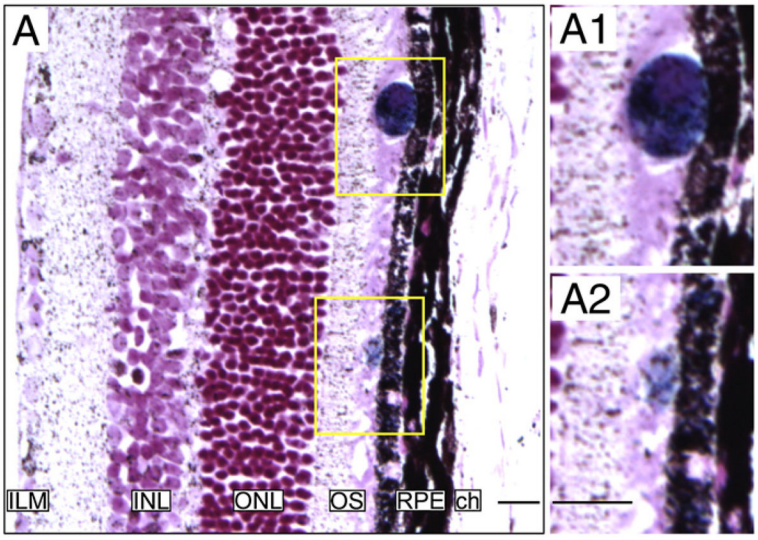

Fig. 7.

Histological detection of injected cells in mouse eyes. A: Section of a mouse retina injected with MION-labeled cells. MION positive cells were detected by Prussian blue staining. Forty-eight hours post-injection some cells appeared to have reached the outer segment (OS) and some of them appeared incorporated into the retinal pigmented epithelium (RPE). Higher magnification images are shown (A1 and A2). ILM: Inner Limiting Membrane; INL: Inner Nuclear Layer; ONL: Outer Nuclear Layer; ch: Choroid.

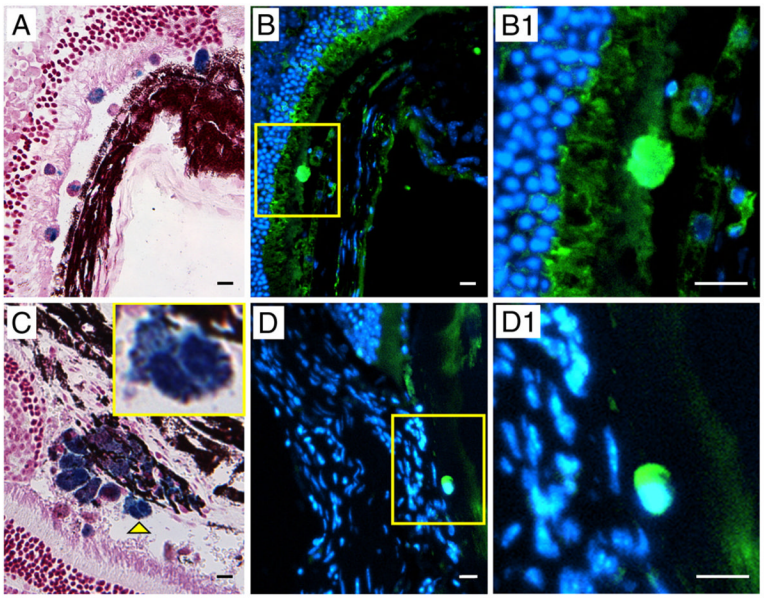

Fig. 8.

Histological identification of injected MION-labeled cells in mouse eyes. A: MION-labeled cells were detected by Prussian Blue staining. B: Injected cells were identified as of human origin as shown by immunoreactivity with antibodies against human nuclear antigen (green) (B) and human CD34 (green) (D). C: Another tissue section showing MION-labeled cells detected by Prussian Blue staining. Yellow arrowhead points at a dividing cell shown at higher magnification in the inset. B1 and D1: Higher magnification of cells depicted in the yellow boxes in panels B and D, respectively.